Cell Biochem Biophys (2016) 74:459–472
DOI 10.1007/s12013-016-0761-6

ORIGINAL PAPER

Biochemical Characterization of the Detoxifying Enzyme Glutathione Transferase P1-1 from the Camel *Camelus Dromedarius*

Fereniki Perperopoulou[1] · Farid S. Ataya[2,3] · Dalia Fouad[4,5] · Ajamaluddin Malik[2,6] · Hesham Mahmoud Saeed[7] · Nikolaos E. Labrou[1]

Received: 11 May 2016 / Accepted: 26 August 2016 / Published online: 17 September 2016

Abstract Glutathione transferase (GST, EC 2.5.1.18) is a primary line of defense against toxicities of electrophile compounds and oxidative stress and therefore is involved in stress-response and cell detoxification. In the present study, we investigated the catalytic and structural properties of the glutathione transferase (GST) isoenzyme P1-1 from *Camelus dromedarius* (*Cd*GSTP1-1). Recombinant *Cd*GSTP1-1 was produced in *Escherichia coli* BL21(DE3) and purified to electrophoretic homogeneity. Kinetic analysis revealed that *Cd*GSTP1-1 displays broad substrate specificity and shows high activity towards halogenated aryl-compounds, isothiocyanates and hydroperoxides. Computation analysis and structural comparison of the catalytic and ligand binding sites of *Cd*GSTP1-1 with other pi class GSTs allowed the identification of major structural variations that affect the active site pocket and the catalytic mechanism., Affinity labeling and kinetic inhibition studies identified key regions that form the ligandin-binding site (L-site) and gave further insights into the mechanism of non-substrate ligand recognition. The results of the present study provide new information into camelid detoxifying mechanism and new knowledge into the diversity and complex enzymatic functions of GST superfamily.

Keywords Glutathione transferase · Kinetic analysis · One-humped camel · Xenobiotics

Abbreviations

*Cd*GSTP1-1	glutathione transferases from *Camelus dromedaries*
BCNB	1-bromo-2,4-dinitrobenzene
CDNB	1-chloro-2,4-dinitrobenzene
CuOOH	cumene hydroperoxide
DHAR	dehydroascorbate
FDNB	1-fluoro-2,4-dinitrobenzene
Fluorodifen	4-nitrophenyl 2-nitro-4-trifluoromethylphenylether
G-site	glutathione binding site
GSH	glutathione
GST	glutathione transferase
HED	2-hydroxyethyl disulfide
H-site	hydrophobic binding site
IDNB	1-iodo-2,4-dinitrobenzene
pNPA	p-nitrophenyl acetate
PEITC	phenylisothiocyanate
ROS	reactive oxygen species

✉ Nikolaos E. Labrou
lambrou@aua.gr

[1] Laboratory of Enzyme Technology, Department of Biotechnology, School of Food, Biotechnology and Development, Agricultural University of Athens, 75 Iera Odos Street, Athens GR-11855, Greece

[2] Department of Biochemistry, College of Science, King Saud University, P.O. Box 2455, Riyadh 11451, Saudi Arabia

[3] Molecular Biology Department, Genetic Engineering Division, National Research Centre, 33 El-Bohouth St. (former El-Tahrir St.), P.O. 12622, Dokki, Giza, Egypt

[4] Department of Zoology, College of Science, King Saud University, P.O. Box 22452, Riyadh 11459, Saudi Arabia

[5] Department of Zoology and Entomology, Faculty of Science, Helwan University, Ein Helwan, Cairo, Egypt

[6] Protein Research Chair, Department of Biochemistry, College of Science, King Saud University, PO Box 2455, Riyadh 11451, Saudi Arabia

[7] Department of Biotechnology, Institute of Graduate Studies and Research, Alexandria University, Alexandria, Egypt

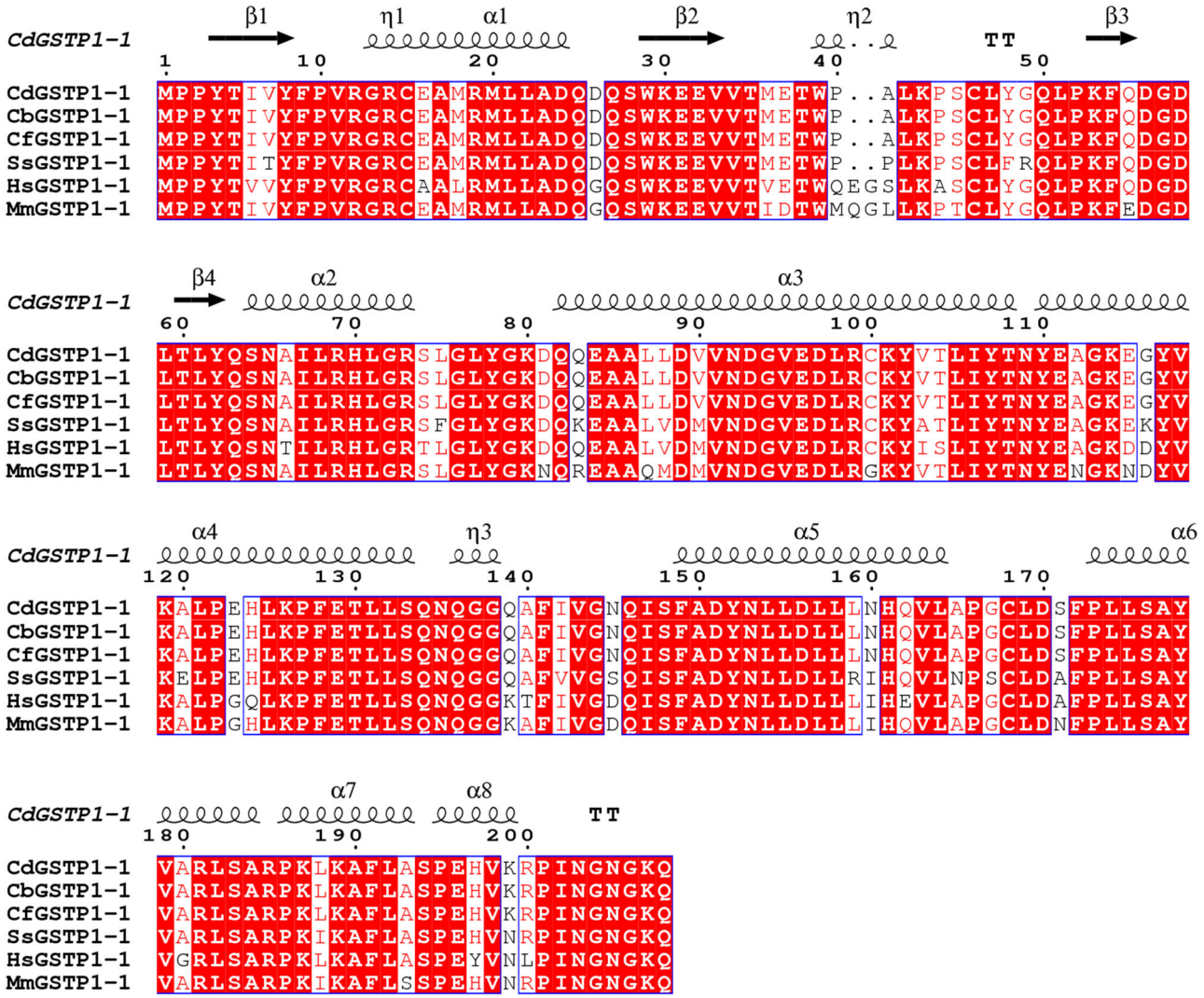

Fig. 1 Multiple sequence alignment of *Cd*GSTP1-1 homologues enzymes. The alignments were produced using Clustal Omega [55]. The program ESPript 3.0 was used for alignment visualization. *Cd*GSTP1-1 numbering is shown above the alignment. Alpha helices and beta strands are represented as helices and arrows, respectively, and beta turns are marked with TT. Conserved areas are shown shaded. A column is framed, if more than 70 % of its residues are similar according to physico–chemical properties. NCBI accession numbers for GSTs are in brackets: GST from *Camelus dromedarius* (*Cd*GSTP1-1, AHN49805.1), *Camelus bactrianus* (*Cb*GSTP1-1, XP_010955041), *Camelus ferus* (*Cf*GSTP1-1, EPY87515.1), *Mus musculus* (*Mm*GSTP1-1, NP_038569), *Sus scrofa* (*Ss*GSTP1-1, XP_005660679), *Homo sapiens* (*Hs*GSTP1-1, CAA30847.1)

Introduction

Living cells are exposed to many life-threatening agents like xenobiotics and reactive oxygen species (ROS) that affect the proteome and genome stability. A specific detoxification mechanism has been evolved to inactivate such toxic compounds through two phases; activation (phase I) and detoxification (phase II). Glutathione transferases (GSTs; EC 2.5.1.18) consist a large multi-functional family belonging to phase II [1]. They are classified into three main families: cytosolic (cGST), mitochondrial (mGST) and membrane-bound microsomal GSTs (MGSTs) [2]. In mammals, cGSTs are classified into seven distinct classes termed: alpha (GSTA), mu (GSTM), omega (GSTO), pi (GSTP), sigma (GSTS), theta (GSTT) and zeta (GSTZ) [3]. Members of these classes catalyze the conjugation of the reduced glutathione (γ-Glu–Cys–Gly, GSH) to electrophilic xenobiotic substrates converting them to less toxic and more water-soluble forms [1–6]. All cGSTs are homodimeric enzymes. Each subunit consists of two domains and have one active site per subunit. Domain I is situated at the N-terminal and has an α/β topology. This part of enzyme forms the GSH binding site (G-site). Domain II is situated at the C-terminal region and adopts an all α helical structure. Domain I and domain II form the GSH binding

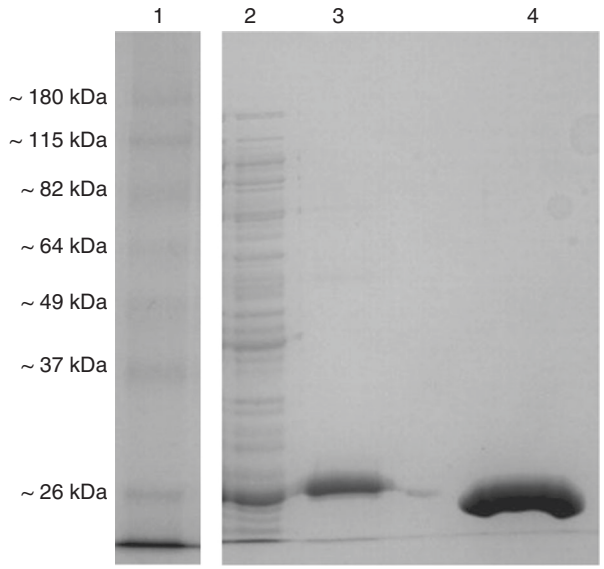

Fig. 2 SDS-PAGE analysis of purified *Cd*GSTP1-1 enzyme. Lane 1: molecular weight markers. Lane 2: crude extract of *E. coli* BL21(DE3) expressing *Cd*GSTP1-1. Lane 3: eluted fraction from the Ni-NTA affinity column, Lane 4: eluted fraction from the GSH-Sepharose affinity column after digestion by thrombin

site (G-site) and the hydrophobic binding site (H-site), respectively [1–3].

Mammalian GSTP1-1 is an important soluble cytosolic enzyme that exhibits many different biological functions. The enzyme is involved in protecting organisms towards the toxicity of xenobiotics as well as their metabolites [7]. For instance, it has been proved that the absence of certain GST isozymes is an indicator of sensitivity to specific cancers [8], and GSTpi null mice are prone to carcinogen-induced tumorigenesis [9]. Besides the detoxification catalytic function of GSTP1-1, it also plays an important noncatalytic roles in cell survival, stress signaling mechanisms [10, 11] and glutathionylation of cellular proteins [12]. Human GSTP1-1 can inhibit the apoptotic c-jun N-terminal kinase (JNK) through protein–protein interactions [13], and is able to form complexes with other proteins that are involved in redox regulation [14]. The S-glutathionylation reaction regulates the catalytic activity and biological function of several proteins. In addition to the catalytic functions, GSTP1-1 is able to bind a diverse range of non-substrate ligands (ligandin function) [6, 15–18]. This ligandin ability is known to affect enzymatic activity.

The one-humped camel, *Camelus dromedarius*, lives in the Arabian Peninsula under harsh desert condition and is exposed to both intrinsic metabolic products and extrinsic environmental stress conditions. Saudi camels represent 16 % of the total animal biomass [19], and have high economic value since are the main source of meat. Therefore, functional genomics of camelid genes that are involved in antioxidant and detoxification mechanisms and contribute to the animal stress response and adaptation is very important research area. In the present work, we describe the expression and biochemical characterization of the recombinant GSTP1-1 from *C. dromedarius* (*Cd*GSTP1-1). The results of this work contribute towards a better understanding on camel adaptation in desert conditions.

Materials and Methods

Expression in *Escherichia coli* BL21(DE3) and Purification of *Cd*GSTP1-1

The codons corresponding to *Cd*GSTP1-1 were optimized (Genescript, USA) for expression in *E. coli* maintaining identical aminoacid sequence (Genbank Database accession number: KJ128390). Two restriction sites, *Bam*HI and *Xho*I were added to the coding region and subcloned in the expression vector pET28a(+) (Novagen, Inc. Madison, USA) under the control of T7 promotor and kanamycin resistance gene for selection. The fidelity and orientation of the clone gene were confirmed by nucleotide sequencing using the T7 primers. The recombinant plasmid [pET-28a(+)*Cd*GSTP1-1] was used to transform *E. coli* BL-21(DE3). The cells were cultured in 1 L LB medium containing 25 µg/mL kanamycin and incubated at 37 °C. The expression of *Cd*GSTP1-1 from *E. coli* BL-21 (DE3) was induced using isopropyl 1-thio-β-galactopyranoside (IPTG) (1 mM) when the absorbance (600 nm) was about 0.6. After induction (approximately 4 h), the culture was centrifuged (8000 g, 10 min). The cell pellet was resuspended in 1.5 mL of lysis buffer (50 mM potassium phosphate buffer, pH 8.0, containing 300 mM NaCl and 10 mM imidazole). The suspension was sonicated and centrifuged at 13,000 g for 5 min. The clear supernatant was used for enzyme purification on Ni-NTA adsorbent (1 mL). The adsorbent was previously equilibrated with lysis buffer. After extract loading, the column was washed off with 10 mL equilibration buffer, followed by 6 mL of wash buffer (50 mM potassium phosphate buffer, pH 8.0, containing 300 mM NaCl, pH 8). Elution of *Cd*GSTP1-1 was achieved with equilibration buffer containing imidazole (0.25 M, 2 mL). Total protein was determined using the Bradford assay [20]. The 6His tag was excised by thrombin (PBS buffer, 5 units thrombin/mg protein, incubation 4 h). Following digestion, the enzyme was separated from the tag by affinity chromatography on GSH-Sepharose column (1,4-butanediol diglycidyl ether-GSH-Sepharose-CL6B). The mixture was loaded to the column (1 mL) which was previously equilibrated with potassium phosphate buffer (20 mM,

Table 1 Substrate specificity for purified recombinant *Cd*GSTP1-1

Substrate	Structure	Specific activity (%)
1-Chloro-2,4-dinitrobenzene	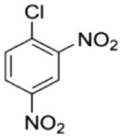	100
p-Nitrobenzyl chloride	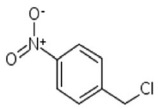	30.5
Fluorodifen	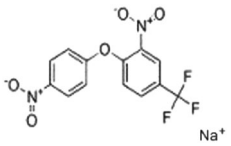	1.2
Bromosulfophthalein	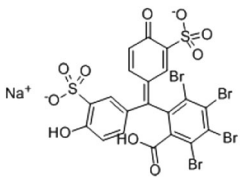	ND
4-Chloro-7-nitrobenzofurazan	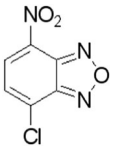	8.2
2,3-Dichloro-4-[2-methylene-butyryl] phenoxy)acetic acid (Ethacrynic acid)	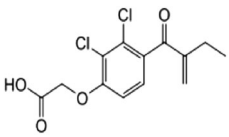	ND
Dehydroascorbate	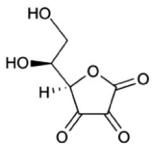	43.6
Sulphanilamide	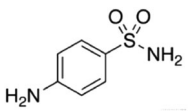	81.8
trans-4-Phenyl-3-buten-2-one	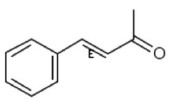	1.2
trans-2-Nonenal	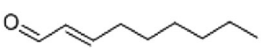	5.9

Table 1 continued

Substrate	Structure	Specific activity (%)
Cumene hydroperoxide	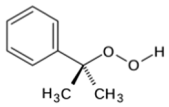	56.3
tert-Butyl hydroperoxide	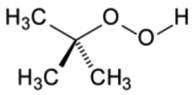	ND
Benzoyl peroxide	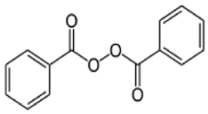	ND
Allyl isothiocyanate	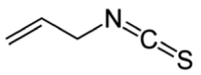	58.9
Phenethyl isothiocyanate (PEITC)	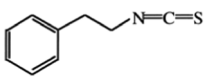	129.7
2-Hydroxyethyl disulfide (2,2-dithiodiethanol)	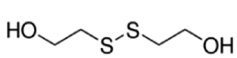	ND

Enzyme assays were carried out under standard conditions as described in Methods section. Results represent the means of triplicate determinations, with variation less than 5 % in all cases

[a] ND: Non-detectable

pH 7). Non-adsorbed protein was washed off with 10 mL equilibration buffer. Bound *Cd*GSTP1-1 was eluted with equilibration buffer containing GSH (10 mM). The purity of the protein was determined by 12.5 % SDS-PAGE according to the method of Laemmli (1970) [21], and the gel was stained by Coomassie Brilliant Blue R-250.

Assay of Enzyme Activity, Protein Determination and Kinetic Analysis

Enzyme assays and protein concentration were measured as described in [22–28]. Kinetic analysis was carried out as follows: initial velocities were determined at saturated concentration of GSH (2.5 mM) and the electrophile substrate (CDNB, PEITC, CuOOH) was used in the concentration range of (0.1–10) × K_m. Initial velocities were also determined at saturated concentration of the electrophile substrate (CDNB, PEITC, CuOOH) and GSH was used in the concentration range of (0.1–10) × K_m. The Michaelis-Menten equation was fitted to the steady-state data by nonlinear regression analysis using the GraFit 3 (Erithacus Software Ltd) computer program.

Table 2 Steady-state kinetic analysis of *Cd*GSTP1-1 for the substrate systems: CDNB/GSH, PEITC/GSH and CuOOH/GSH

Substrate System	K_m (mM) (GSH)	K_m (mM) (Xenobiotic substrate)	k_{cat} (min^{-1})	k_{cat}/K_m ($mM^{-1}min^{-1}$) (CDNB)
CDNB/GSH	0.45 ± 0.02	4.5 ± 0.35	277 ± 13	61.6
PEITC/GSH	0.25 ± 0.02	0.047 ± 0.01	180 ± 15	3846
CuOOH/GSH	0.12 ± 0.01	14.3 ± 3.6	542 ± 118	37.9

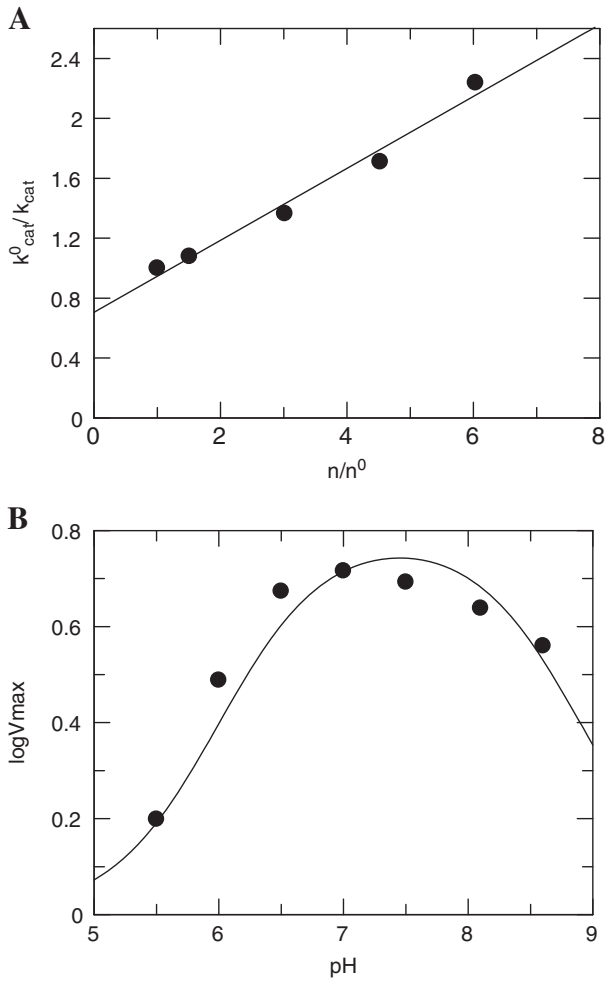

Fig. 3 **a** The effect of viscosity on k_{cat} for the CDNB-GSH reaction. Plot of the reciprocal of the relative turnover number (k°_{cat}/k_{cat}) as a function of relative viscosity (η/η°) with glycerol as cosolvent. Lines were calculated by least-squares regression analysis. **b** Dependence of $\log V_{max}$ on pH for the CDNB-GSH catalytic reaction. Buffer used was 0.1 M potassium phosphate

Enzyme Inactivation Studies

Inactivation of *Cd*GSTP1-1 was performed in potassium phosphate buffer pH 7.0 (20 mM, 1 mL), containing Vilmafix blue A-R (VBAR) (10 µM); enzyme, (1 unit). The time course of inactivation was followed by periodically removing samples for assay of enzymatic activity. Inactivation studies of *Cd*GSTP1-1 by VBAR in the presence of S-nitrobenzyl-GSH or epoxiconazole were performed in 1 mL of incubation mixture containing: potassium phosphate buffer pH 7.0 (20 mM); VBAR, (10 µM); S-nitrobenzyl-GSH (1 mM) or epoxiconazole (100 µM); enzyme (1 unit). The inactivation data were fitted to the pseudo first-order equation:

$$A = A_0 e^{-k_{inact}t}$$

where k_{inact} is the observed rate of enzyme inactivation (min^{-1}), and A is the enzyme activity at a specific time t and A_0 is the initial enzyme activity.

Thermal Stability of the *Cd*GSTP1-1 and Inhibition Analysis

Thermal inactivation of the *Cd*GSTP1-1 was carried out as described in [27, 29]. The melting temperature (T_m) was determined from the plot of relative inactivation (%) versus temperature (°C). The kinetics of thermal inactivation of the *Cd*GSTP1-1 was monitored at 4, 12, 37, and 45 °C. Inactivation rates were determined from plots of remaining enzyme activity vs. time (min) according to equation:

$$\text{Remaining activity} = (1 - F)e^{-k_{fast}t} + Fe^{-k_{slow}t}$$

where F is the fraction of the remaining enzyme and k_{fast} and k_{slow} are the rate constants for the slow and fast phases of the reaction, respectively.

The thermal stability of *Cd*GSTP1-1 was also investigated using Differential Scanning Fluorimetry in the presence of Protein Thermal Shift™ Dye (Applied Biosystems). The enzyme (0.71 µg) was added in potassium phosphate buffer pH 6.5 and was mixed with the dye. Protein samples were run in triplicate on an Applied Biosystems® real-time PCR StepOne™ instrument. The temperature gradient that was used for fluorescence monitoring was 25–65 °C, at a rate of 1 °C/min. The melting point of the enzyme (T_m) was determined by the Protein Thermal Shift™ Analysis Software and Boltzmann equation was fitted to the experimental data.

Analysis of the inhibition potency of different xenobiotic compounds (pesticides) towards *Cd*GSTP1-1 was accomplished as described in [27, 28].

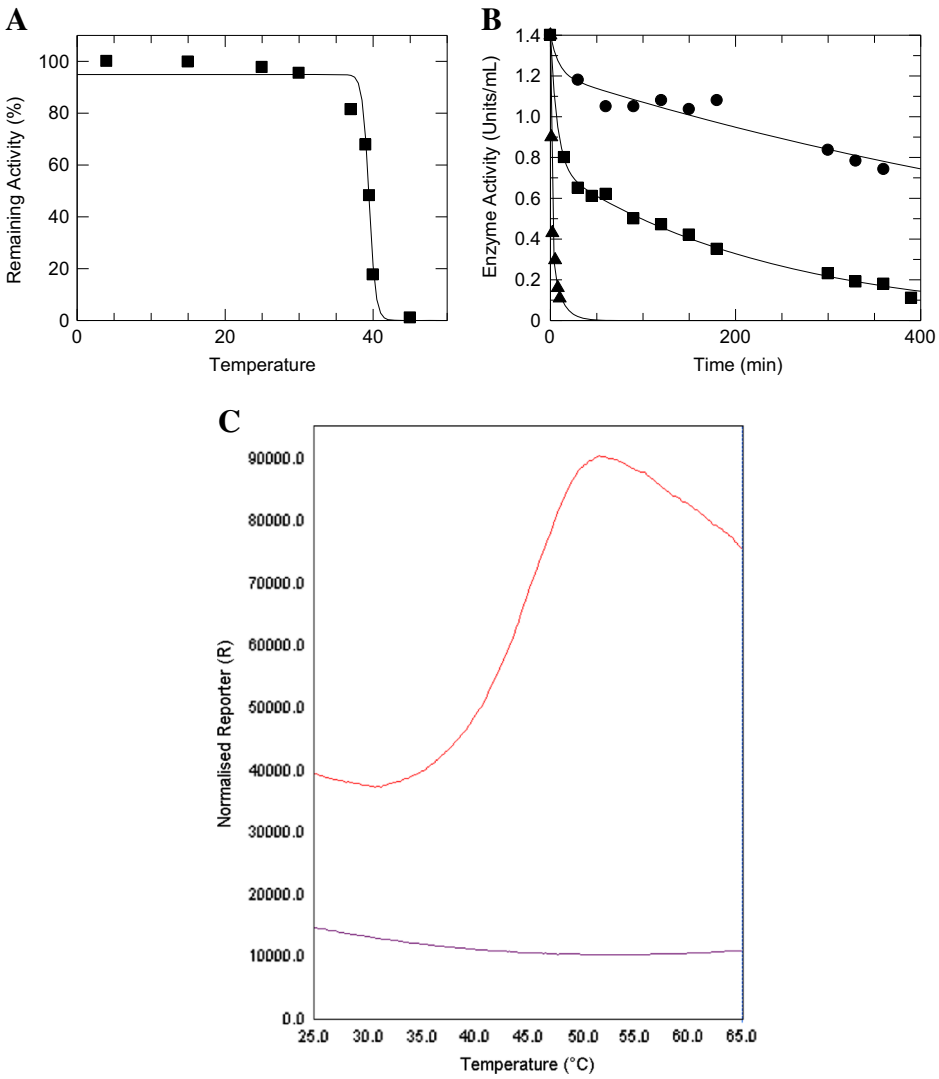

Fig. 4 **a** Thermal inactivation curve. The residual activity of *Cd*GSTP1-1 was measured after heat treatment at various temperatures (°C) for 5 min. **b** Kinetics of thermal inactivation. The residual activities of the enzyme were measured at various times after incubation at different temperatures: 25 °C (●), 37 °C (■), 45 °C (▲). **c**. Thermal denaturation curve (upper line) and response of control sample (lower line) for *Cd*GSTP1-1 using differential scanning fluorimetry

Table 3 Inactivation rates for the fast and slow phases

Temperature (°C)	k_{fast} (min^{-1}) ($\times 10^{-4}$)	k_{slow} (min^{-1}) ($\times 10^{-4}$)
4	1.3	1.1
12	20.3	5.0
25	111.6	12.2
37	133.3	41.3
45	735.4	96.7

Viscosity and pH Dependence of Kinetic Parameters

The effect of viscosity on k_{cat} was studied in 0.1 M potassium phosphate buffer, pH 6.5, containing variable glycerol concentrations, as described in [27–34]. Analysis of the pH dependence of V_{max} was carried out as described in [27, 29].

Bioinformatic Analysis and Molecular Modeling

The molecular model of *Cd*GSTP1-1 was constructed using SWISS-MODEL [35]. The available crystal structure of GST that was used as template for model construction was 2oac (PDB code) (*Mus musculus* GST, 87.92 % homology with *Cd*GSTP1-1). The Global Model Quality Estimation score was estimated 0.98 and QMEAN score for the estimation of the global and local model quality −1.43, suggesting high quality of the model. For inspection of models and crystal structures the programs PyMOL (http://www.pymol.org/) [36] and UCSF Chimera were used. CastP server (http://sts.bioengr.uic.edu/castp/calculation.php) [37] was employed for measuring putative pockets. Conserved pockets analyses were carried out using Hpocket [38]. The program ESPript 3.0 (run at http://espript.ibcp.fr/ESPript/cgi-bin/ESPript.cgi) was utilized for alignment visualization and manipulation.

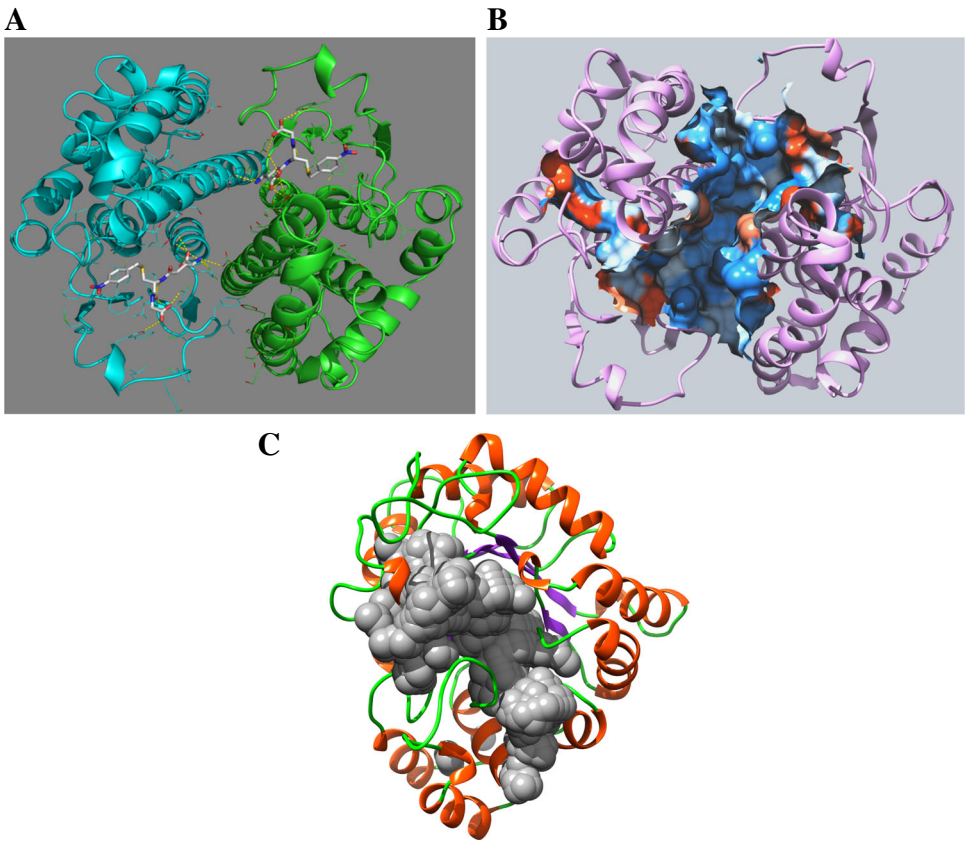

Fig. 5 **a** Carton representations of *Cd*GSTP1-1 model. Bound ligand (*S*-nitrobenzyl-GSH) is shown in a stick representation. Putative hydrogen bonds are shown as yellow dashed-lines. The picture was created by PyMOL. **b** The hydrophobicity surface of the larger pocket of *Cd*GSTP1-1 model as calculated by CASTp [37]. The picture was created by UCSF Chimera. **c** Conserved pocket analyses in homologues proteins using the Hpocket algorithm [38]. The conserved pocket extracted from homologues structures (PDB) is shown in a spheres representation and colored grew. The picture was created by UCSF Chimera

The putative binding sites of epoxiconazole and Vilmafix blue A-R (VBAR) were identified by molecular-docking using the SwissDock program and EADock DSS software [39]. The docking was performed with no region of interest defined (blind docking). Default values were used during docking. CHARMM energies were measured and binding modes are evaluated using FACTS, and clustered [40].

Results and Discussion

Heterologous Expression of *Cd*GSTP1-1 in *E. coli* BL21 (DE3) and Purification

Figure 1 shows the amino acid sequence alignments resulting from the BLASTp search of *Cd*GSTP1-1 sequence. CdGSTP1-1 displays high homology with other well characterized pi class enzymes from other organisms such as *Homo sapiens* (86.54 %), *Mus musculus* (88.46 %) and *Sus scrofa* (90.38 %). The catalytically important amino acid residue Tyr8 [41] (numbering according to *Cd*GSTP1-1) as well as other residues that affect substrate binding and catalysis (e.g., Arg14, Cys46, Tyr48, Tyr110) are all conserved [31, 42].

The coding sequences of *Cd*GSTP1-1 was cloned and expressed as 6His-tag fusion protein in *E. coli* BL21(DE3) under T7 promotor of pET-28a(+) vector. The recombinant enzyme was purified to electrophoretic homogeneity (>98 % purity, Fig. 2) by affinity chromatography on Ni-NTA-agarose column, followed by GSH-Sepharose column.

Substrate Specificity of *Cd*GSTP1-1

The specificity of *Cd*GSTP1-1 was investigated using a panel of substrates and the results are listed in Table 1. *Cd*GSTP1-1 displays activity towards eleven out of sixteen different electrophilic compounds that were evaluated. In general, *Cd*GSTP1-1 accepts as substrates halogenated aryl-compounds such as 1-chloro-2,4-dinitrobenzene (CDNB) and p-nitrobenzyl chloride (pNBC). Steady-state kinetic analysis of *Cd*GSTP1-1 using the substrate system CDNB/GSH was carried out and the kinetic constants are listed in Table 2. The K_m value of *Cd*GSTP1-1 for GSH (0.45 mM) is close to that measured for the human GSTP1-1 enzyme (K_m 0.27 mM) [42]. However, the K_m^{CDNB} for *Cd*GSTP1-1 (4.5 mM) is about 5.6-times higher, compared to the human enzyme [42]. The K_m values for GSH (Table 2) are dependent on the electrophilic substrate used and vary within a relative narrow range (0.12–0.45 mM).

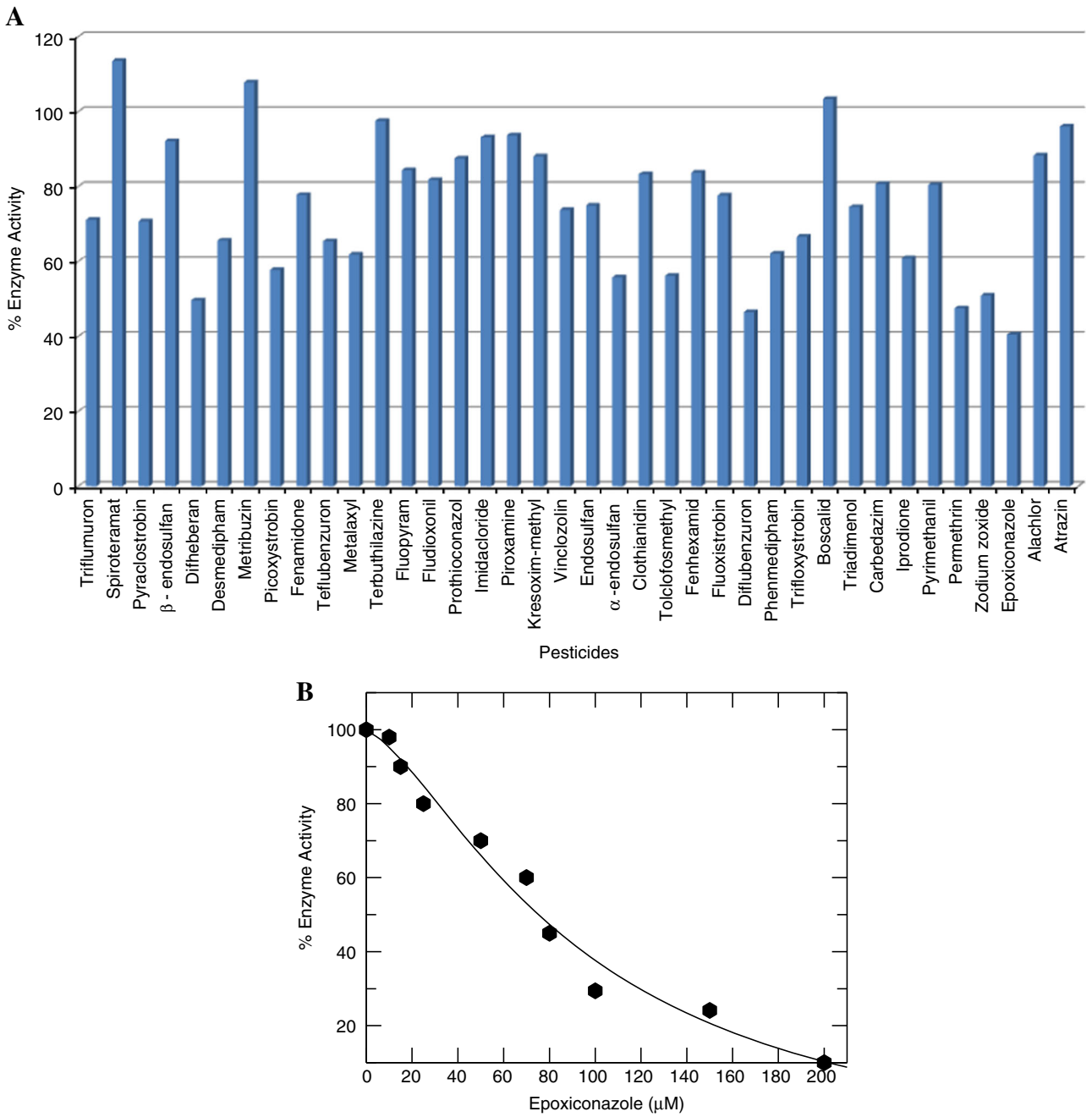

Fig. 6 **a** Screening of inhibition potency of selected pesticides (100 μM) towards *Cd*GSTP1-1. *Cd*GSTP1-1 was assayed in all measurements using the CDNB–GSH assay system. **b** Dose-response inhibition of *Cd*GSTP1-1 by epoxiconazole. Enzyme assays were carried out using CDNB–GSH as substrates

*Cd*GSTP1-1 displays GSH-dependent hydroperoxidase activity. Among three differed hydroperoxides tested (cumene hydroperoxide, tert-butyl hydroperoxide, and benzoyl-peroxide), only cumene hydroperoxide was acceptable substrate by *Cd*GSTP1-1. The k_{cat} and K_m values for cumene hydroperoxide were determined as 542 min^{-1} and 14.3 mM, respectively (Table 2). In addition to GSH-peroxidase activity, several GST isoenzymes also show dehydroascorbate reductase and thioltransferase activity [23, 43]. *Cd*GSTP1-1 catalyzes the reduction of dehydroascorbate (Table 1) but does not show thioltransferase activity.

*Cd*GSTP1-1 accepts as substrates unsaturated carbonyl compounds such as nonenal and *trans*-4-phenyl-3-buten-2-one (Table 2). Unsaturated carbonyls are cytotoxic compounds that are produced by lipid peroxidation and are detoxified by GSTs via Michael addition reaction [6, 27–30, 44, 45]. Isothiocyanates are plant substances that are

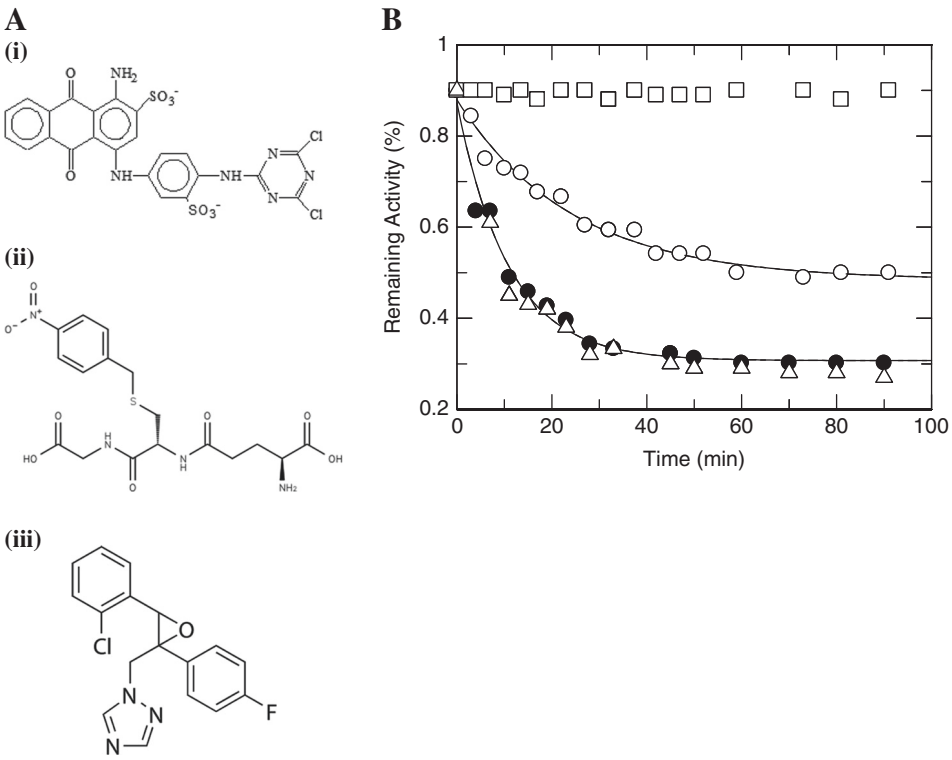

Fig. 7 Probing the ligandin-binding site of *Cd*GSTP1-1 by affinity labeling. **a**. The structures of: VBAR (i); *S*-nitrobenzyl-glutathione (ii); and epoxiconazole (iii). **b** Inactivation of *Cd*GSTP1-1 by VBAR at pH 7.0 and 25 °C. Enzyme was incubated in the absence of VBAR (□); in the presence of VBAR (10 μM) (•); in the presence of VBAR (10 μM) and S-nitrobenzyl-GSH (1 mM) (○); in the presence of of VBAR (10 μM) and epoxiconazole (100 μM) (Δ). At the times indicated, aliquots were withdrawn and assayed for enzymatic activity

Table 4 Energies (FullFitness, kcal/mol and ΔG, kcal/mol) of the predicted binding modes of epoxiconazole and VBAR in two main binding sites of *Cd*GSTP1-1

Ligand	Binding site	FullFitness (kcal/mol)	ΔG (kcal/mol)
Epoxiconazole	Intersubunit cleft	−1357.6	−6.5
	Overlap G- and H-site	−1355.8	−7.2
VBAR	Intersubunit cleft	−1705.3	−10.5
	Overlap G- and H-site	−1703.1	−8.4

released, as a response to stress, after hydrolysis of glucosinolates [46]. *Cd*GSTP1-1 catalyzes the conjugation of GSH to the isothiocyanate group of allyl-isothiocyanate and phenethyl-isothiocyanate. With phenethyl-isothiocyanate as substrate, *Cd*GSTP1-1 displays the highest catalytic efficiency (k_{cat}/K_m) (Table 2), 62-times and 102-times higher compared to the CDNB/GSH and CuOOH/GSH reaction systems, respectively. This suggests that isothiocyanates may represent a group of compounds that are "natural" substrates for *Cd*GSTP1-1 in vivo.

Effect of Viscosity and pH on the Kinetic Parameters of *Cd*GSTP1-1

The effect of viscosity on k_{cat} for the CDNB/GSH conjugation reaction was studied for obtaining information on the rate-limiting step (Fig. 3a) [27–30, 42]. As presented in Fig. 3a the plot of $k_{cat}°/k_{cat}$ on $\eta/\eta°$ is linear (R^2 0.9897) with a slope 0.24 ± 0.02, showing that the rate-limiting step is affected by viscosity-dependent motions or conformational changes of the enzyme. This is in agreement with the results observed for the human GSTP1-1 enzyme. In this case the rate-limiting step is a physical event, relevant to a structural transition of the ternary complex [34].

The pH dependence of V_{max} for *Cd*GSTP1-1 was investigated to shine light on the ionizable residues that play roles in substrate binding and catalysis (Fig. 3b). The results showed that the pH dependence of V_{max} displays a bell-shaped trend, with two clear inflection points that correspond to an apparent $pK_{a1} = 6.0 \pm 0.2$ and $pK_{a2} = 8.4 \pm 0.20$. It is well known that GSTs catalytic performance is accomplished by lowering the pK_a of the –SH group of the bound GSH, thus improving its nucleophilicity [31, 41, 47, 48]. In the pi class GSTs this is achieved by the active site residue Tyr8 (Fig. 1), whose hydroxyl group is in hydrogen bond with the –SH group of bound GSH [41]. Published work shows that the pK_a of –SH group of bound GSH ranges from 6.0 to 6.5 as calculated for the human GSTP1-1 enzyme and other GST-GSH binary complexes [29, 31, 41]. It is conceivable that the observed pK_{a1} may reflect the ionization of the thiol group of the bound GSH in *Cd*GSTP1-1. On the other hand the pK_{a2} is close to the value expected for a Lys or Cys residues that may be involved in substrate binding and/or catalysis [29].

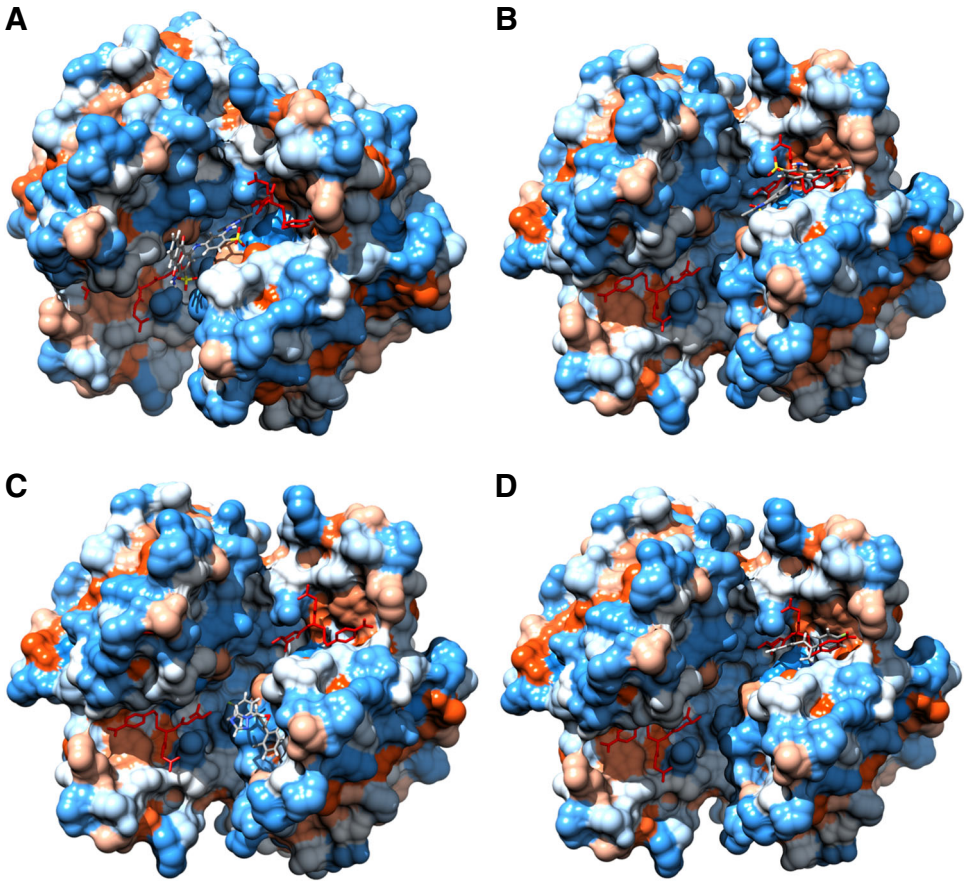

Fig. 8 **a** The predicted favorable binding mode of VBAR and *Cd*GSTP1-1. VBAR is shown in stick representation and colored according to atom type. Bound *S*-nitrobenzyl-GSH is depicted in a stick representation and colored red. *Cd*GSTP1-1 model is shown by hydrophobicity surface. **b** The predicted less favorable binding mode of VBAR and *Cd*GSTP1-1. VBAR is depicted in stick representation and colored according to atom type. Bound *S*-nitrobenzyl-GSH is depicted in a stick representation and colored red. *Cd*GSTP1-1 model is shown by hydrophobicity surface. **c** The predicted favorable binding mode of epoxiconazole and *Cd*GSTP1-1. The epoxiconazole is shown in stick representation and colored according to atom type. *Cd*GSTP1-1 model is depicted by hydrophobicity surface. Bound *S*-nitrobenzyl-GSH is shown in a stick representation and colored red. **d** The predicted less favorable binding mode of epoxiconazole and *Cd*GSTP1-1. The epoxiconazole is shown in stick representation and colored according to atom type. *Cd*GSTP1-1 model is depicted by hydrophobicity surface. Bound *S*-nitrobenzyl-GSH is shown in a stick representation and colored red

Thermal Stability of *Cd*GSTP1-1

The inactivation profile of *Cd*GSTP1-1 (Fig. 4a, Table 3) showed one transition with inflection point corresponding to half-inactivation temperature (T_m) of 39.4 ± 0.1 °C. Kinetic analysis of the inactivation process of the enzyme between 4 °C–45 °C gave biphasic kinetics with a rapid inactivation occurring immediately and a slow inactivation continuing longer (Fig. 4b) [49, 50]. This suggests that at the initial stage a fraction of the enzyme is rapidly inactivated (fast step) while the remainder is converted (slow step) into a modified yet active form, whose subsequent inactivation is slower. The inactivation rates for the fast and slow phases are listed in Table 3. The proportion of activity lost by the rapid process seems to be strongly dependent on temperature because the k_{fast} is more responsive to changes in temperature than is k_{slow} (Table 3). The kinetics of *Cd*GSTP1-1 inactivation appears to be different compared to the human P1-1 enzyme which obeyed first-order kinetics and higher thermostability [42].

The thermal stability of *Cd*GSTP1-1 was also investigated using differential scanning fluorometry [18] and the results are shown in Fig 4c. The denaturation profile exhibits a single transition with an asymmetric peak, with maximum fluorescence intensity at 52 °C. The decrease in fluorescence on the right-hand side of the peak is typically due to aggregation and precipitation of the denatured protein, as well as to the natural decrease in quantum yield of the fluorescent dye at higher temperatures [51]. A T_m of 41.7 °C was obtained with high reproducibility, very close to that found in Fig. 4a.

Characterization the Ligandin-binding Site (L-site) of *Cd*GSTP1-1 by Computation Analysis and Affinity Labeling Experiments

Certain GSTs are considered as high-capacity binding proteins (ligandins) for a wide range of non-substrate compounds. These compounds bind to the ligandin-binding site (L-site). This ability of GSTs contributes in several ligand-uptake, ligand-transport and ligand-storage functions [15, 16]. Crystallographic work on porcine pi class GST in complex with 8-anilino-1-naphthalenesulfonic acid and bromosulfophthalein showed that these compounds bind to the same surface site which is located outside of H- and G-site and formed by Trp28, Trp38, Cys45 [52]. Oakley et al. showed that in the human GST P1-1 enzyme the L-site is located into the H-site [15]. The results of another work suggested the presence of an expansive L-site that spanned the intersubunit cleft and the H-site in human GST P1-1 enzyme [16]. Therefore, multiple binding modes for ligandin-type compounds may exist in pi class enzymes [53].

In the present work, to assess the presence of a putative L-site in the *Cd*GSTP1-1 enzyme, computation analysis, kinetic inhibition, and affinity labeling experiments were used. The 3D molecular model of *Cd*GSTP1-1 was constructed by homology modeling (Fig. 5a). The homology model was analyzed by CASTp [37] for searching large binding pockets and cavities. The results showed the presence of one large pocket with area 2097.7 A^2 and volume 3243.3 A^3 which overlaps both the G- and H-site and extended in the intersubunit cleft (Fig. 5b). The other pockets identified were surface exposed and significant smaller (< 258.3 A^2 area and 464.1 A^3 volume). Conserved pockets analyses in other homologues proteins using the Hpocket algorithm [38] suggest that this large pocket is conserved along the GST family of enzymes (Fig. 5c).

To further characterize the non-substrate ligand binding features of *Cd*GSTP1-1, the interaction of different xenobiotic compounds (insecticides, fungicides, and herbicides) with the enzyme was studied. This was achieved by measuring the inhibition of *Cd*GSTP1-1 by the selected xenobiotic compounds (Fig. 6), since the binding of non-substrate ligands to the L-site of GSTs usually inhibit their catalytic activity [15, 27, 28, 54]. From the results presented in Fig. 6 it is apparent that *Cd*GSTP1-1 exhibits a rather reduced ability to bind xenobiotic compounds in a non-substrate manner, compared to other GST isoenzymes [27, 28]. Pesticides with one aromatic ring (e.g., alachlor, atrazin) displayed low or no inhibition. On the other hand, bulky compounds with two aromatic rings (e.g., epoxiconazole, permethrin, diflubenzuron) display higher inhibition. Among all tested compounds, epoxiconazole showed the highest inhibition potency with IC_{50} 94.8 ± 5.2 μM.

To further characterize the non-substrate ligand binding features of *Cd*GSTP1-1, the interaction of the reactive anthraquinone dye Vilmafix Blue A-R (VBAR) with *Cd*GSTP1-1 was investigated (Fig. 7). VBAR is an anthraquinone dichlorotriazinyl-dye which is able to interact irreversibly and with high affinity with several GSTs. For example, VBAR has been used as a probe of the L-site of human GSTP1-1 [15] and phi class *Zm*GST1-1 [54]. When *Cd*GSTP1-1 was incubated with VBAR (10 μM) the enzyme was progressively inactivated (Fig. 7). In the absence of VBAR, virtually no change in activity was observed when the enzyme was incubated under identical conditions. The inactivation rate equals to $k_{inact} = 0.0920 \pm 0.0078$ min^{-1}.

The ability of specific ligands to influence the inactivation rate can be taken as evidence of the specificity of the chemical modification reaction [54]. Therefore, the effect of S-nitrobenzyl-glutathione (similar to the reaction product that overlaps both the G- and H-site) on the reaction of VBAR with *Cd*GSTP1-1 was studied. Inactivation of *Cd*GSTP1-1 by VBAR (10 μM) in the presence of S-nitrobenzyl-glutathione results in significant lower inactivation rate ($k_{inact} = 0.0414 \pm 0.0044$ min^{-1}, about 55 % lower), suggesting that VBAR competes with S-nitrobenzyl-glutathione for binding in the same site in *Cd*GSTP1-1. On the other hand, the inactivation rate of *Cd*GSTP1-1 by VBAR in the presence of epoxiconazole remained unaltered (Fig. 7b). This implies that VBAR and epoxiconazole do not compete for binding in the same site of the enzyme, suggesting the presence of two putative L-sites.

In silico molecular docking studies were carried out to analyze the interaction of VBAR and epoxiconazole with *Cd*GSTP1-1. Molecular docking of VBAR and epoxiconazole resulted in 32 and 37 clusters that corresponded to two different sub-sites within the large pocket that identified by CASTp and Hpocket analysis (Fig. 5). The FullFitness score [39, 40] and energy (ΔG, kcal/mol) of the top-score clusters are listed in (Table 4). All other clusters had a significantly lower FullFitness score and ΔG. The most favorable binding mode of VBAR and epoxiconazole with *Cd*GSTP1-1, which correspond to top-score clusters, are shown in Figs. 8a and c, respectively. Analysis of the putative binding sites suggests that the binding of VBAR and epoxiconazole to the enzyme may be mainly accomplished by hydrophobic interaction that provides the driving force for positioning and recognition of these compounds by *Cd*GSTP1-1. VBAR binds at a distinct position in the intersubunit cleft that partially contacts the G-site. This confirms the competition of VBAR and S-nitrobenzyl-glutathione observed in the affinity labeling experiment (Fig. 7). On the other hand, the in silico study predicts that epoxiconazole binds to a different site at the entrance of the large pocket (Fig. 8c). This binding mode allows

simultaneously the accommodation of both the VBAR and the epoxiconazole, confirming the lacks of competition observed in the affinity labeling experiment (Fig. 7).

An alternative binding mode was also observed, in which VBAR and epoxiconazole bind in a different location, that overlap the G- and H-sites (Figs. 8b and d). However, FullFitness score is less satisfactory (Table 4) and the binding mode appears less favorable since some apolar moieties of the ligands are located in more polar region (G-site). Accordingly, the binding mode showing in Figs. 8a and c should be preferred.

In conclusion, in the present work we report the biochemical characterization of *Cd*GSTP1-1. The results advance our understanding of camelid detoxification and stress response mechanisms. The study of the structure and catalytic function of detoxifying and stress response-related enzymes, such as GSTs, helps on the better understanding of how the camel is adapted to live in desert conditions. In addition, the structural aspects and phylogenetic analysis of GSTs discussed in the present study give further insights into the diversity and evolution of the Phase II metabolizing enzymes in camel.

Acknowledgments The authors (FSA, DF, HMS) extend their appreciation to the King Abdulaziz City for Science and Technology (KACST), Riyadh, Saudi Arabia, for partially funding the work through the project # P.C-32-22.

Compliance with Ethical Standards

Conflict of Interest The authors declare that they have no conflict of interest.

Author Contributions FP, perform experiments and analyzed data; FSA, perform experiments, analyzed data, wrote the paper; DF, perform experiments, analyzed data; HMS, perform experiments, analyzed data; NEL, design experiments, analyzed data, wrote the paper. All authors have approved the final version of the article.

References

1. Labrou, N. E., Papageorgiou, A. C., Pavli, O., & Flemetakis, E. (2015). Plant GSTome: structure and functional role in xenome network and plant stress response. *Current Opinion in Biotechnology*, *32*, 186–194.
2. Hayes, J. D., Flanagan, J. U., & Jowsey, I. R. (2005). Glutathione S-transferases. *Annual Review of Pharmacology and Toxicology*, *4*, 51–88.
3. Mannervik, B. (2012). Five decades with glutathione and the GSTome. *The Journal of Biological Chemistry*, *287*, 6072–6083.
4. Hayes, J. D., & Pulford, D. J. (1995). The glutathione S-transferase supergene family: regulation of GST and the contribution of the isoenzymes to cancer chemoprotection and drug resistance. *Critical Reviews in Biochemistry and Molecular Biology*, *30*, 445–600.
5. Eaton, D. L., & Bammler, T. K. (1999). Concise review of the glutathione S-tarnsferases and their significance to toxicity. *Toxicological Sciences : An Official Journal of the Society of Toxicology*, *49*, 156–164.
6. Board, P. G., & Menon, D. (2013). Glutathione transferases, regulators of cellular metabolism and physiology. *Biochimica et Biophysica Acta*, *1830*, 3267–3288.
7. Sun, N., Sun, X., Chen, B., Cheng, H., Feng, J., Cheng, L., & Lu, Z. (2010). MRP2 and GSTP1 polymorphisms and chemotherapy response in advanced non-small cell lung cancer. *Cancer Chemotherapy and Pharmacology*, *65*, 437–446.
8. Henderson, C. J., Smith, A. G., Ure, J., Brown, K., Bacon, E. J., & Wolf, C. R. (1998). Increased skin tumorigenesis in mice lacking pi class glutathione S-transferases. *Proceedings of the National Academy of Sciences USA*, *95*, 5275–5280.
9. Salinas, A. E., & Wong, M. G. (1999). Glutathione S-transferases: a review. *Current Medicinal Chemistry*, *6*, 279–309.
10. Wu, Y., Fan, Y., Xue, B., Luo, L., Shen, J., Zhang, S., Jiang, Y., & Yin, Z. (2006). Human glutathione S-transferase P1-1 interacts with TRAF2 and regulates TRAF2-ASK1 signals. *Oncogene*, *25*, 5787–5800.
11. Sánchez-Gómez, F. J., Díez-Dacal, B., Pajares, M. A., Líorca, O., & Pérez-Sala, D. (2010). Cyclopentenone prostaglandins with dienone structure promote cross-linking of the chemoresistance-inducing enzyme glutathione transferase P1-1. *Molecular Pharmacology*, *78*, 723–733.
12. Townsend, D. M., Manevich, Y., He, L., Hutchens, S., Pazoles, C. J., & Tew, K. D. (2009). Novel role for glutathione S-transferase pi. Regulator of protein S-Glutathionylation following oxidative and nitrosative stress. *The Journal of Biological Chemistry*, *284*, 436–445.
13. Federici, L., Lo Sterzo, C., Pezzola, S., Di Matteo, A., Scaloni, F., Federici, G., & Caccuri, A. M. (2009). Structural basis for the binding of the anticancer compound 6-(7-nitro-2,1,3-benzoxadiazol-4-ylthio)hexanol to human glutathione s-transferases. *Cancer Research*, *69*, 8025–8034.
14. Manevich, Y., Feinstein, S. I., & Fisher, A. B. (2004). Activation of the antioxidant enzyme 1-CYS peroxiredoxin requires glutathionylation mediated by heterodimerization with pi GST. *Proceedings of National Academy of Sciences USA*, *101*, 3780–3785.
15. Oakley, A. J., Lo Bello, M., Nuccetelli, M., Mazzetti, A. P., & Parker, M. W. (1999). The ligandin (non-substrate) binding site of human Pi class glutathione transferase is located in the electrophile binding site (H-site). *Journal of Molecular Biology*, *291*, 913–926.
16. Oakley, A. J., Rossjohn, J., Lo Bello, M., Caccuri, A. M., Federici, G., & Parker, M. W. (1997). The three-dimensional structure of the human Pi class glutathione transferase P1-1 in complex with the inhibitor ethacrynic acid and its glutathione conjugate. *Biochemistry*, *36*, 576–585.
17. Mahajan, S., & Atkins, W. M. (2005). The chemistry and biology of inhibitors and prodrugs targeted to glutathione S-transferases. *Cellular and Molecular Life Sciences : CMLS*, *62*, 1221–1233.
18. Lea, W. A., & Simeonov, A. (2012). Differential scanning fluorometry signatures as indicators of enzyme inhibitor mode of action: case study of glutathione S-transferase. *PLoS One*, *7*(4), e36219.
19. Al-Swailem, A. M., Shehata, M. M., Abu-Duhier, F. M., Al-Yamani, E. J., Al-Busadah, K. A., Al-Arawi, M. S., Al-Khider, A. Y., Al-Muhaimeed, A. N., Al-Qahtani, F. H., Manee, M. M., Al-Shomrani, B. M., Al-Qhtani, S. M., Al-Harthi, A. S., Akdemir, K. C., Inan, M. S., & Out, H. H. (2010). Sequencing, analysis, and annotation of expressed sequence tags for *Camelus dromedaries*. *PLoS One*, *5*(5), e10720.
20. Bradford, M. M. (1976). A rapid and sensitive method for the quanti- fication of microgram quantities of protein utilizing the

principle of protein-dye binding. *Analytical Biochemistry*, *72*, 248–254.
21. Laemmli, U. K. (1970). Cleavage of structural proteins during the assembly of the head of bacteriophage T4. *Nature*, *227*, 680–685.
22. Habig, W. H., Pabst, M. J., & Jakoby, W. B. (1974). Glutathione S-transferases. The first enzymatic step in mercapturic acid formation. *The Journal of Biological Chemistry*, *249*, 7130–7139.
23. Chronopoulou, E., Madesis, P., Asimakopoulou, B., Platis, D., Tsaftaris, A., & Labrou, N. E. (2012). Catalytic and structural diversity of the fluazifop-inducible glutathione transferases from *Phaseolus vulgaris*. *Planta*, *235*, 1253–1269.
24. Axarli, I., Labrou, N. E., Petrou, C., Rassias, N., Cordopatis, P., & Clonis, Y. D. (2009). Sulphonamide-based bombesin prodrug analogues for glutathione transferase, useful in targeted cancer chemotherapy. *European Journal of Medicinal Chemistry*, *44*(5), 2009–2016.
25. Kolm, R. H., Danielson, U. H., Zhang, Y., Talalay, P., & Mannervik, B. (1995). Isothiocyanates as substrates for human glutathione transferases: structure-activity studies. *The Biochemical Journal*, *311*, 453–459.
26. Allocati, N., Favaloro, B., Masulli, M., Alexeyev, M. F., & Di Ilio, C. (2002). *Proteus mirabilis* glutathione S-transferase B1-1 is involved in protective mechanisms against oxidative and chemical stresses. *The Biochemical Journal*, *373*, 305–311.
27. Chronopoulou, E., Madesis, P., Tsaftaris, A., & Labrou, N. E. (2014). Cloning and characterization of a biotic-stress-inducible glutathione transferase from *Phaseolus vulgaris*. *Applied Biochemistry and Biotechnology*, *172*, 595–609.
28. Chronopoulou, E., Papageorgiou, A., Markoglou, A., & Labrou, N. E. (2012). Inhibition of human glutathione transferases by pesticides: development of a simple analytical assay for the quantification of pesticides in water. *Journal of Molecular Catalysis B Enzymatic*, *81*, 43–51.
29. Skopelitou, K., Muleta, A. W., Papageorgiou, A. C., Chronopoulou, E., & Labrou, N. E. (2015). Catalytic features and crystal structure of a tau class glutathione transferase from *Glycine max* specifically upregulated in response to soybean mosaic virus infections. *Biochimica et Biophysica Acta*, *1854*, 166–177.
30. Skopelitou, K., Dhavala, P., Papageorgiou, A. C., & Labrou, N. E. (2012). A glutathione transferase from *Agrobacterium tumefaciens* reveals a novel class of bacterial GST superfamily. *PLoS One*, *7*, e34263.
31. Labrou, N. E., Mello, L. V., & Clonis, Y. D. (2001). Functional and structural roles of the glutathione-binding residues in maize *(Zea mays)* glutathione S-transferase I. *The Biochemical Journal*, *358*, 101–110.
32. Pouliou, F. M., Thireou, T. N., Eliopoulos, E. E., Tsoungas, P. G., Labrou, N. E., & Clonis, Y. D. (2015). Isoenzyme- and allozyme-specific inhibitors: 2,2'-dihydroxybenzophenones and their carbonyl N-analogues that discriminate between human glutathione transferase A1-1 and P1-1 allozymes. *Chemical Biology & Drug Design*, *86*, 1055–1063.
33. Axarli, I., Dhavala, P., Papageorgiou, A. C., & Labrou, N. E. (2009). Crystallographic and functional characterization of the fluorodifen-inducible glutathione transferase from *Glycine max* reveals an active site topography suited for diphenylether herbicides and a novel L-site. *Journal of Molecular Biology*, *385*, 984–1002.
34. Caccuri, A. M., Ascenzi, P., Antonini, G., Parker, M. W., Oakley, A. J., Chiessi, E., Nuccetelli, M., Battistoni, A., Bellizia, A., & Ricci, G. (1996). Structural flexibility modulates the activity of human glutathione transferase P1-1. Influence of a poor co-substrate on dynamics and kinetics of human glutathione transferase. *The Journal of Biological Chemistry*, *271*, 16193–16198.
35. Arnold, K., Bordoli, L., Kopp, J., & Schwede, T. (2006). The SWISS-MODEL Workspace: a web-based environment for protein structure homology modeling. *Bioinformatics (Oxford, England)*, *22*, 195–201.
36. DeLano, W. L. (2002). *The PyMOL Molecular graphics system*. CA, USA: DeLano scientific San Carlos.
37. Dundas, J., Ouyang, Z., Tseng, J., Binkowski, A., Turpaz, Y., & Liang, J. (2006). CASTp: computed atlas of surface topography of proteins with structural and topographical mapping of functionally annotated residues. *Nucleic Acids Research*, *34*, W116–W118.
38. Le Guilloux, V., Schmidtke, P., & Tuffery, P. (2009). Fpocket: an open source platform for ligand pocket detection. *BMC Bioinformatics*, *10*, 168.
39. Grosdidier, A., Zoete, V., & Michielin, O. (2011). SwissDock, a protein-small molecule docking web service based on EADock DSS. *Nucleic Acids Research*, *39*, W270–W277.
40. Grosdidier, A., Zoete, V., & Michielin, O. (2007). EADock: docking of small molecules into protein active sites with a multiobjective evolutionary optimization. *Proteins*, *67*, 1010–1025.
41. Kong, K. H., Takasu, K., Inoue, H., & Takahashi, K. (1992). Tyrosine-7 in human class Pi glutathione S-transferase is important for lowering the pKa of the thiol group of glutathione in the enzyme-glutathione complex. *Biochemical and Biophysical Research Communications*, *184*, 194–197.
42. Zimniak, P., Nanduri, B., Pikuła, S., Bandorowicz-Pikuła, J., Singhal, S. S., Srivastava, S. K., Awasthi, S., & Awasthi, Y. C. (1994). Naturally occurring human glutathione S-transferase GSTP1-1 isoforms with isoleucine and valine in position 104 differ in enzymic properties. *European Journal of Biochemistry / FEBS*, *224*, 893–899.
43. Chronopoulou, E. G., & Labrou, N. E. (2009). Glutathione transferases: emerging multidisciplinary tools in red and green biotechnology. *Recent Patents on Biotechnology*, *3*, 211–223.
44. Hegazy, U. M., Mannervik, B., & Stenberg, G. J. (2004). Functional role of the lock and key motif at the subunit interface of glutathione transferase p1-1. *The Journal of Biological Chemistry*, *279*, 9586–9596.
45. Ye, Z. W., Zhang, J., Townsend, D. M., & Tew, K. D. (2015). Oxidative stress, redox regulation and diseases of cellular differentiation. *Biochimica et Biophysica Acta*, *1850*, 1607–1621.
46. Dosz, E. B., Ku, K. M., Juvik, J. A., & Jeffery, E. H. (2014). Total myrosinase activity estimates in brassica vegetable produce. *Journal of Agricultural and Food Chemistry*, *62*, 8094–8100.
47. Axarli, I., Dhavala, P., Papageorgiou, A. C., & Labrou, N. E. (2009). Crystal structure of Glycine max glutathione transferase in complex with glutathione: investigation of the mechanism operating by the Tau class glutathione transferases. *The Biochemical Journal*, *422*, 247–256.
48. Deponte, M. (2013). Glutathione catalysis and the reaction mechanisms of glutathione-dependent enzymes. *Biochimica et Biophysica Acta*, *1830*, 3217–3266.
49. Sturtevant, J. M. (1987). Biochemical applications of differential scanning calorimetry. *Annual Review of Physical Chemistry*, *38*, 463–488.
50. Freire, E., Van Osdol, W. W., Mayorga, O. L., & Sanchez-Ruiz, J. M. (1990). Calorimetrically determined dynamics of complex unfolding transitions in proteins. *Annual Review of Biophysics and Biophysical Chemistry*, *19*, 159–188.
51. Krasavin, M., Stavniichuk, R., Zozulya, S., Borysko, P., Vullo, D., & Supuran, C. T. (2016). Discovery of Strecker-type α-aminonitriles as a new class of human carbonic anhydrase inhibitors using differential scanning fluorimetry. *Journal of Enzyme Inhibition and Medicinal Chemistry*, *16*, 1–5.

52. Bico, P., Erhardt, J., Kaplan, W., & Dirr, H. (1995). Porcine class-pi glutathione S-transferase – anionic ligand-binding and conformational analysis. *Biochimica et Biophysica Acta*, *1247*, 225–230.
53. Van Zanden, J. J., Hamman, O. B., Van Iersel, M. L., Boeren, S., Cnubben, N. H., Lo Bello, M., Vervoort, J., Van Bladeren, P. J., & Rietjens, I. M. (2003). Inhibition of human glutathione S-transferase P1-1 by the flavonoid quercetin. *Chemico-biological Interactions*, *145*, 139–148.
54. Axarli, I. A., Rigden, D. J., & Labrou, N. E. (2004). Characterization of the ligandin site of maize glutathione S-transferase I. *The Biochemical Journal*, *382*, 885–893.
55. Sievers, F., Wilm, A., Dineen, D. G., Gibson, T. J., Karplus, K., Li, W., Lopez, R., McWilliam, H., Remmert, M., Söding, J., Thompson, J. D., & Higgins, D. (2011). Fast, scalable generation of high-quality protein multiple sequence alignments using Clustal Omega. *Molecular Systems Biology*, *7*, 539.